Compressed Streak Imaging Beam Diagnostic*

D. Marks[ξ], D. Frayer
National Security Technologies, LLC, New Mexico Operations, Los Alamos Office
182 East Gate Drive, Los Alamos, NM 87544, USA

Abstract

We are planning a new beam diagnostic based on Compressed Ultrafast Photography (CUP)[1]. A foil inserted in the beam path is used to generate a continuous optical image of the beam, which is the same technique used on the existing DARHT II beam imaging diagnostic. This existing diagnostic compresses the beam image with anamorphic lenses into four views that are streaked simultaneously on two streak cameras. In our new beam diagnostic design the anamorphic lenses are replaced with regular lenses and the beam image is stamped with a pseudo-random mask pattern. The full image is imaged onto a streak camera with its entrance slit expanded. Modifying the CUP technique, which uses a single streaked image, our design splits the image into four rotated copies and puts all four images on two streak cameras. A data cube of multiple image frames is reconstructed from the streak camera data through the use of the TwiST algorithm[2] combined with total variation denoising[3]. The additional rotated images improve spatial resolution and reduce noise and image artifacts compared to using a single streaked image. In reconstructions of simulated data, fine detail in the beam profile can be seen and there is a remarkable absence of image artifacts compared to the existing DARHT II beam imaging diagnostic. Performance was evaluated using a pseudo-MTF derived from a simulated wave pattern test object.

I. INTRODUCTION

Beam diagnostics played a fundamental role in the commissioning and optimization of the Dual-Axis Radiographic Hydrodynamic Test (DARHT) facility linear induction accelerators at Los Alamos National Laboratory[4,5]. These flash x-ray radiographic machines provide single and multi-pulse radiographs of hydrodynamic experiments. In conjunction with beam-positioning sensors and beam energy diagnostics, the beam imaging system[6,7] on DARHT II has helped greatly with the tuning of this multi-pulse accelerator to meet stringent beam requirements.

This paper describes a proposed beam imaging diagnostic that combines the optical transition radiation (OTR) foil used on the existing DARHT II beam imaging diagnostic with a powerful new compressed sensing technique called Compressed Ultrafast Photography (CUP). In CUP, a time series of images are compressed onto the image output of a streak camera by first stamping the image with an unchanging pseudo-random mask pattern before it reaches the front photocathode of the streak camera. An iterative reconstruction technique with a strong total variation prior is used to reconstruct the three-dimensional data cube from the streak camera image.

This paper is organized into the following sections. Section II describes the proposed construction of the system. Section III describes the reconstruction method for generating the time-series of images from a set of images generated by the streak cameras. Section IV presents the results of our simulations, including a method used to evaluate system performance. Section V is a discussion of the results and presents other applications of the technique.

II. SYSTEM DESIGN

A diagram of the proposed beam imaging system is shown in Fig. 1. The electron beam strikes an OTR foil to generate on optical image of the beam. The existing beam imaging diagnostic on DARHT II uses 1mm titanium foils or sometimes aluminum coated quartz. If the beam is well focused the beam diameter will be ~1 mm, but the main value of this diagnostic is for tuning defocused beams, in which case the beam diameter will be much larger.

* This manuscript has been authored by National Security Technologies, LLC, under Contract No. DE AC52-06NA25946 with the U.S. Department of Energy and supported by the Site-Directed Research and Development Program. The United States Government retains and the publisher, by accepting the article for publication, acknowledges that the United States Government retains a non-exclusive, paid-up, irrevocable, world-wide license to publish or reproduce the published form of this manuscript, or allow others to do so, for United States Government purposes. The U.S. Department of Energy will provide public access to these results of federally sponsored research in accordance with the DOE Public Access Plan (http://energy.gov/downloads/doe-public-access-plan). DOE/NV/25946--2488.
ξ email: MarksDG@nv.doe.gov

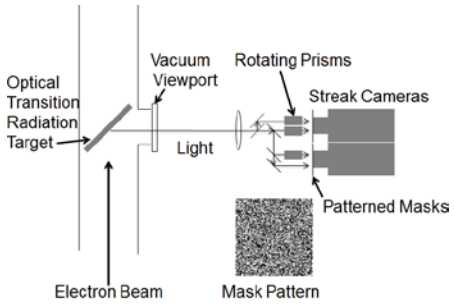

Figure 1. Diagram of proposed beam imaging diagnostic with four rotated images on two streak cameras.

The light emitted from the OTR target passes through a vacuum viewport and is then split into four copies with beam splitters and mirrors after passing through a lens system (only a single lens is shown in the diagram). Three of the images have rotating prisms that rotate 45º, 90º and 135º. The path lengths for the four images can be made equal but this is not necessary if the depth of field is made sufficiently large. We assume a target angle of 45º in our simulations and have not included any imperfections due to the optical system. We have also assumed that the unequal magnification of the electron beam in *x* and *y* will be removed by the optical system, but an exact optical system design has not been done.

Mask patterns on glass or plastic are placed at the front surface of the photocathode on the streak cameras. These are pseudo-random block patterns. It was found that the optimum size for the smallest blocks is close to the resolution element size of the streak camera. We use a 128×128 block pattern for each image which is then mapped to a 256×256 image on the CCD of the streak camera. The block pattern is different for each of the four images. We model the blur in the streak camera as a Gaussian blur with FWHM of 50 μm, with magnification of 1.0 from the photocathode to the CCD and a 1024×1024 CCD with 25 μm pixels. Appropriate signal-dependent noise was included in our system model, with the assumption that the highest counts on the CCD will be ¼ of the maximum counts.

There are several alternative arrangements of the system that could have some advantages. Two viewing angles could be used, allowing for more light collection and reducing the number of beam splitters. If one of the streak cameras is rotated 90º then one rotating prism could be eliminated. The existing DARHT II beam imaging diagnostic uses fiber arrays to carry the signals far from the beam line, reducing radiation on the cameras. Our proposed diagnostic could use imaging fiber bundles, but this is an expensive addition. We are assuming the diagnostic will sit adjacent to the beam line, requiring extra shielding.

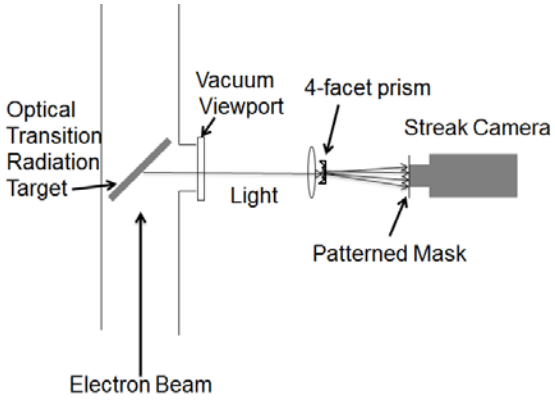

Figure 2. Diagram of alternative beam imaging diagnostic with four images split from a single prism without rotations.

We have also considered a system that does not use rotating prisms, as shown in Fig. 2. A single 4-facet prism divides the light into four images without any rotation. This is a much simpler system, and it should be able to fit all four images onto one streak camera. The disadvantage is that reconstruction is more complicated and gives poorer results than the system with rotated images.

III. RECONSTRUCTION METHOD

A two-step iterative shrinkage/thresholding (TwIST)[2] algorithm is used to reconstruct the time-series of images from the streak camera data, which is the same method used by the original CUP[1] authors.

The system is modeled as a matrix operation

$$y = \mathbf{K}x + \eta(\mathbf{K}x), \tag{1}$$

where y is the streak camera data, $\mathbf{K}$ is the system transfer matrix, x is the true time series of images and η is the noise operator which is signal-dependent. We have not included the signal-dependent nature of the noise in our consideration of reconstruction algorithms, so this signal-dependence will be ignored. In our simulations of data, however, this signal-dependence is included.

To reconstruct x from f we solve the minimization problem

$$\operatorname{argmin}_x \left\{ \frac{\| \mathbf{K}x - y \|^2}{2} + \lambda \Phi(x) \right\}, \tag{2}$$

where λ is the regularizing parameter and Φ is a constraint function, which in our case is a total-variation constraint.

The total variation constraint Φ uses the discreet forward difference operators ∂_h and ∂_v representing horizontal and vertical differences,

$$\partial_h(i,j) = \begin{cases} x(i+1,j) - x(i,j) & \text{if } i < N, \\ 0 & \text{if } i = N \end{cases} \quad (3)$$

$$\partial_v(i,j) = \begin{cases} x(i,j+1) - x(i,j) & \text{if } j < N, \\ 0 & \text{if } j = N \end{cases}, \quad (4)$$

where the object x is a time series of $N \times N$ images. The total-variation constraint function Φ is

$$\Phi(x) = \sum_{1 \le i,j \le N} \left|\partial_v(i,j)\right| + \left|\partial_h(i,j)\right|. \quad (5)$$

Eqs. (3–5) are not used directly in the reconstruction algorithm. To solve Eq. (2), an iterative backprojection of smoothed residuals is used. The initial guess x_0 has all values initialized to 0, although the algorithm is not sensitive to the choice of x_0. The first iteration is

$$x_1 = \Gamma(x_0), \quad (6)$$

where

$$\Gamma(x) = \Psi\left(x + \mathbf{K}^{\mathrm{T}}(y - \mathbf{K}x)\right) \quad (7)$$

and Ψ is a total-variation denoising operator based on Chambolle's projection algorithm[3,8], which we will not describe here. The remaining iterations are

$$x_{t+1} = (1-\alpha)x_{t-1} + (\alpha - \beta)x_t + \beta\,\Gamma_\lambda(x_t), \quad (8)$$

where α and β are constants. There are techniques[2] for choosing optimum values of α and β. We found empirically that $\alpha = 0.5$ and $\beta = 0.02$ worked well for our system.

An additional constraint was added to ensure positivity in the reconstruction. This was done by forcing all negative values in x_t to zero at the end of each iteration.

It was found that Eq. (8) gave good reconstructions when rotated images were used. When non-rotated images were used, using the system shown in Fig. 2, a severe artifact was found in the appearance of a constant background image that slides down the reconstruction in the sweep direction. One way to fix this problem is to use the first frame of the reconstruction to determine the background and then subtract a sliding version of this background from all of the images. This only works if the first frame has no light in it. We found that the background closely resembled the backprojection of the data, so we instead used the following algorithm to subtract the background,

$$x_{fixed} = x - \tau\, G\left(\mathbf{K}^{\mathrm{T}}(y)\right), \quad (9)$$

where τ is a constant and G is a Gaussian smoothing operator. This correction is applied at the end of the reconstruction and was found intuitively without a theoretical justification. More research is needed to determine why Eq. (9) appears to work and to optimize it. Attempts to incorporate this correction within each iteration of the reconstruction algorithm did not give good results.

IV. RESULTS

A. Simulated Data and Reconstructions

A simulated beam pulse of 60 ns duration was used to test the performance of the system, of which two sample images at different times are shown in Fig. 3. The full field of view was 5 mm as measured at the electron beam, and the maximum width of the beam was 2.7 mm. A complex changing beam profile was used to simulate a defocused beam. The sweep length was 1500 ns, so the sweep travelled one pixel in 1.5 ns. One image frame was reconstructed for each pixel of sweep, so the reconstruction had 40 frames during the pulse with 50 total frames reconstructed.

The streak camera data from the four rotated images, broken out into separate images, is shown in Fig. 4.

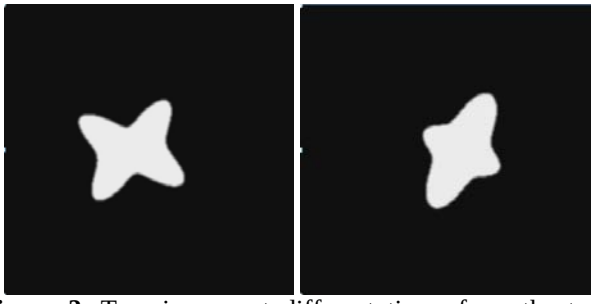

Figure 3. Two images at different times from the test beam pulse used to evaluate the system.

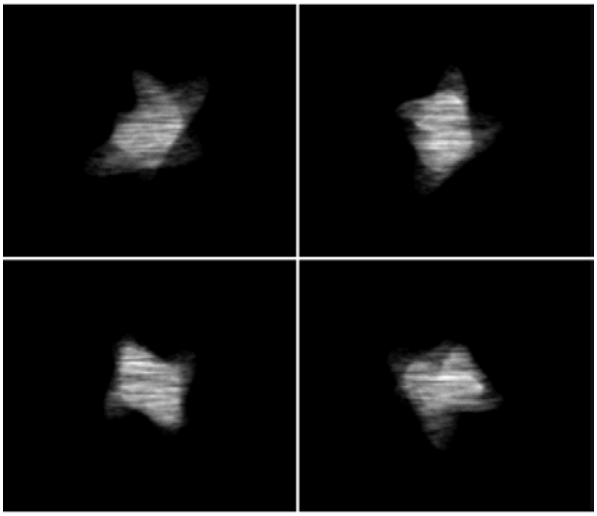

Figure 4. Four streak camera images generated from the beam pulse shown in Fig. 3. The sweep direction is to the right.

The reconstruction from the data shown in Fig. 4 was done using Eqs. (6–8) with 50 iterations of Eq. (8). Two frames from the reconstruction are shown in Fig. 5, corresponding to the times of the frames shown in Fig. 3.

As a comparison, the same object was used to simulate data taken with the existing anamorphic beam diagnostic used on DARHT II, with the results of reconstructions shown in Fig. 6. This diagnostic is useful for getting the general beam size and boundaries, but is unable to reconstruct details of complex beams.

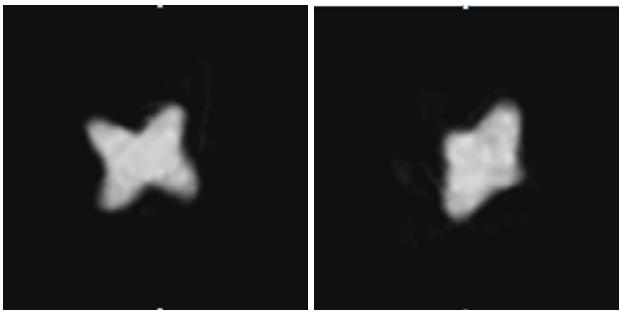

Figure 5. Two images from the reconstruction of the beam from the simulated streak camera data shown in Fig. 4. These are from the same times as the two frames shown in Fig. 3.

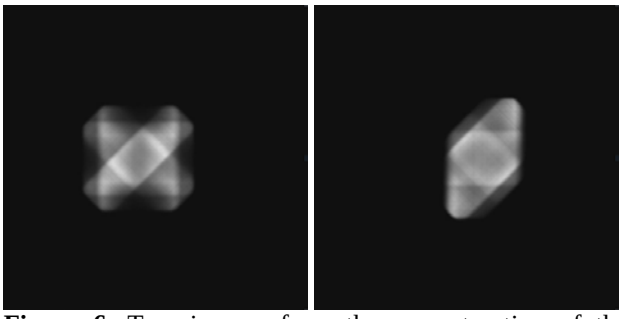

Figure 6. Two images from the reconstruction of the beam from simulations of the existing four-view anamorphic beam diagnostic used on DARHT II.

Simulations were also performed using the non-rotated system from Fig. 2. The results of these reconstructions, including the extra background subtraction step from Eq. (9), are shown in Fig. 7. The background subtraction process does not completely remove the image artifacts and there is a significant increase in noise.

B. Evaluating System Performance

While visual inspections of reconstructions are valuable, there is a need to have an automated method of evaluating system performance. An automated method can be made more objective than visual evaluation and can also be easily performed on large numbers of reconstructions.

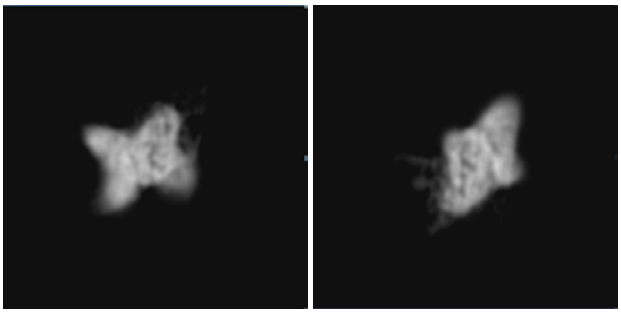

Figure 7. Two images from the reconstruction of the beam from simulations of four non-rotated images using the system shown in Fig. 2.

To automatically evaluate system performance we simulated a test object using a sinusoidal wave pattern, an example of which is shown in Fig. 8. The radius of the object occupies half the field of view. Eight different wavelengths were used and a pseudo-MTF (modulation transfer function) was generated from the modulation in the reconstructions of these wave objects. We call this a pseudo-MTF instead of an MTF because the reconstruction process in non-linear so a traditional MTF is not valid. Instead, the pseudo-MTF gives the modulation transfer for this specific set of test objects, all of which have the same radius. The pseudo-MTF is averaged over test objects rotated at six different angles. The object moves uniformly to the right across the field, always staying in full view. A frame from a reconstruction of the object is shown in Fig. 9.

Figure 8. Test object used to evaluate the pseudo-MTF. This is one of eight frequencies and six rotations that were used.

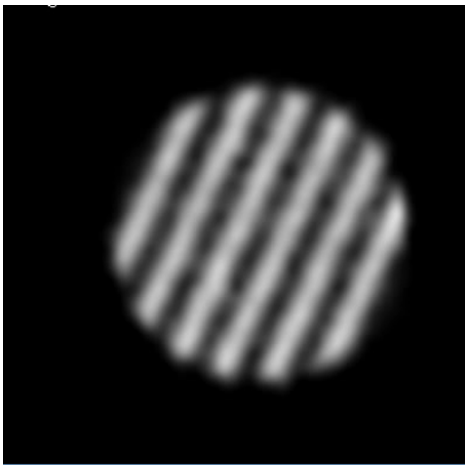

Figure 9. A frame from the reconstruction of the test object from Fig. 8.

We chose the spatial frequency at 25% modulation as our system metric, doing linear interpolation between frequencies to find this point. We can see the value in using this metric in choosing the optimum mask element size. A graph of the 25% modulation point as a function of smallest mask element size is shown in Fig. 10.

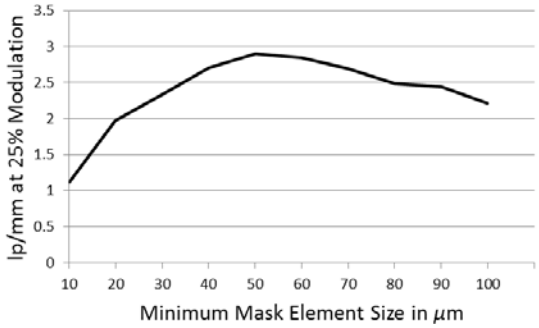

Figure 10. System performance as a function of mask element size, showing that the optimum comes at 50 μm, corresponding to the 128×128 mask pattern that we used. This is also the size of the FWHM of the system blur.

Another example of the use of the pseudo-MTF is seeing how system performance depends on the length of the pulse. We simulated wave objects with different pulse lengths and the results of the pseudo-MTF evaluation are shown in Fig. 11. We see a steady degradation in performance as longer pulses are used. This can be explained by the greater overlap of images as the pulse gets longer. The ratio of reconstructed pixels to data pixels gets larger as more frames are reconstructed, so in essence the data compression is increasing, leading to poorer image quality.

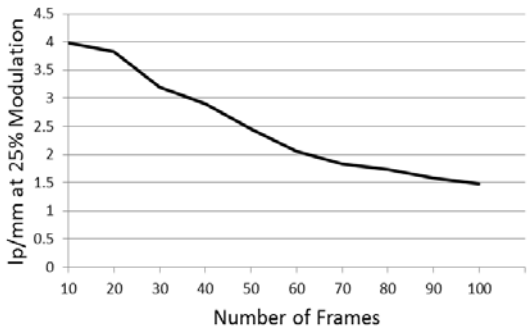

Figure 11. System performance as a function of pulse length expressed as number of reconstructed frames. System performance steadily degrades with increasing numbers of reconstructed frames.

V. DISCUSSION

The modified CUP technique that we have used falls under the general theory of compressed sensing[9] and is very similar to compressed hyperspectral imaging (CHI). CHI also uses a coded mask and a sweep of images across a camera, but with CHI the sweep is in wavelength instead of in time. Much of the theory from CHI applies to CUP, including the degradation in reconstruction quality with greater levels of compression that we see in Fig. 11.

The original use of CUP was for very sparse images where only a small part of the image has data and the object is generally moving so that any one region of the image contains data for very few frames. With the use of multiple images, and particularly with rotated images, the use of CUP can be expanded to data sets that are much less sparse. In our simulations the object is much larger and moves very slowly so each part of the data contributes to many frames of the reconstruction.

The choice between rotating and non-rotating systems will likely be influenced by further improvements in the data analysis. With rotated images, the TwIST algorithm shown in Eqs. (6–8) naturally does a good job of reconstructing the object with little sensitivity to the exact choice of algorithm parameters. With the non-rotating system the results were almost useless unless the background subtraction technique in Eq. (9) is used, and even then the results are significantly worse than when rotations are used. Further work on the reconstruction algorithm may reduce the difference between these two systems and make the non-rotated system preferred due to its greater simplicity.

The fact that data compression increases as the number of reconstructed frames increases imposes limits on this technique's usefulness for analyzing long data records. If the object is smaller and moving quickly across the image, the data compression problem decreases significantly since more pixels in the streak images contain information that can be used in the reconstruction.

We concentrated on objects that moved slowly as a more difficult test of the system performance.

We are considering the development of an x-ray imaging system using the same technique. In the case of x-rays, rotations are not possible when using a single streak camera. A configuration employing two or more rotated cameras could be possible, but this makes an overly complicated system, in addition to introducing significant problems due to using widely spaced viewing angles. We are expecting that the x-ray system will use a single streak camera, so improvement in the analysis of non-rotated images will be very important.

VI. REFERENCES

[1] L. Gao, J. Liang, C. Li and L.V. Wang, "Single-shot compressed ultrafast photography at one hundred billion frames per second," Nature, vol. 516, pp. 74-77, Dec. 4, 2014.

[2] J. M. Bioucas-Dias and M.A.T. Figuerido, "A new TwIST: Two-step iterative shrinkage/thresholding algorithms for image restoration," IEEE Trans. Image Proc., vol. 16, (no. 12), pp. 2992-3004, Dec. 2007.

[3] A. Chambolle, "An algorithm for total variation minimization and applications," J Math. Imaging Vision, vol. 20, pp. 89-97, 2004.

[4] C. Ekdahl, "Modern electron accelerators for radiography," IEEE Trans. Plasma Sci., vol. 30, (no. 1), pp. 254-261, 2002.

[5] C. Ekdahl, "Tuning the DARHT long-pulse linear induction accelerator," IEEE Trans. Plasma Sci., vol. 41, (no. 10), 2774-2780, 2013.

[6] H. Bender, C. Carlson, D. Frayer, D. Johnson, K. Jones, A. Meidinger and C. Ekdahl, "Quasianamorphic optical imaging system with tomographic reconstruction for electron beam imaging," Rev. Sci. Instrum., vol. 78, (no. 1), p. 013301, 2007.

[7] D. Frayer, C. A. Ekdahl and D. Johnson, "Fidelity of a time-resolved imaging diagnostic for electron beam profiles," vol. 42, (no. 10), pp. 2594-2595, Sep. 2014.

[8] J. Duran, B. Coll and C. Sbert, "Chambolle's projection algorithm for total variation denoising," Image Process. On Line, vol. 3, pp. 311-331, 2013.

[9] M. E. Gehm, S. T. McCain, N. P. Pitsianis, D. J. Brady, P. Potuluri, and M. E. Sullivan, "Static two-dimensional aperture coding for multimodal, multiplex spectroscopy," Appl. Opt., vol. 45, (no.13), pp. 2965-2974, 2006.